applied sciences

MDPI

Article

Radiocarbon Dating of Magnesian Mortars: The Case of San Salvatore Church in Massino Visconti, Piedmont, Italy

Giulia Ricci [1,2,*], Michele Secco [2,3], Fabio Marzaioli [4], Isabella Passariello [4], Filippo Terrasi [4] and Gilberto Artioli [1,2]

[1] Dipartimento di Geoscienze, Università di Padova, 35131 Padova, Italy
[2] Centro CIRCe, Università di Padova, 35131 Padova, Italy; michele.secco@unipd.it
[3] Dipartimento dei Beni Culturali (DBC), Università di Padova, 35139 Padova, Italy
[4] Dipartimento di Matematica e Fisica, Università della Campania "Luigi Vanvitelli", 81020 Caserta, Italy; filippo.terrasi@unicampania.it (F.T.)
* Correspondence: giulia.ricci@unipd.it

Abstract: This study presents a comprehensive analysis and radiocarbon dating of historical mortar and plaster samples from the San Salvatore—Massino Visconti complex in Piedmont, Northern Italy. Mortar samples and one charcoal sample were collected from various areas within the complex's lower chapels. Samples were selected and characterized by means of a multi-analytical approach in order to draw inferences about their compositional, mineralogical, and microstructural features. The identification of hydromagnesite and magnesite in the mortar samples suggests the usage of magnesian binder mortar, potentially affecting radiocarbon dating due to its slower carbonation kinetics when compared to calcitic mortars. To mitigate this effect, a purification method was developed involving thermal treatment at 550 °C to isolate datable binding fractions. The results yielded reliable radiocarbon ages consistent with historical context, shedding light on construction materials dating from the 12th to 16th centuries. The study also challenges previous notions by demonstrating the feasibility of radiocarbon dating for magnesian mortars, opening new perspectives for dating such materials. These findings offer valuable insights into the construction history and material composition of the complex, corroborating historical information.

Keywords: ^{14}C dating; accelerator mass spectrometry; magnesian mortars; mortar characterization; hydromagnesite; magnesite

check for updates

Citation: Ricci, G.; Secco, M.; Marzaioli, F.; Passariello, I.; Terrasi, F.; Artioli, G. Radiocarbon Dating of Magnesian Mortars: The Case of San Salvatore Church in Massino Visconti, Piedmont, Italy. *Appl. Sci.* **2024**, *14*, 9899. https://doi.org/10.3390/app14219899

Academic Editor: Asterios Bakolas

Received: 11 September 2024
Revised: 17 October 2024
Accepted: 22 October 2024
Published: 29 October 2024

Copyright: © 2024 by the authors. Licensee MDPI, Basel, Switzerland. This article is an open access article distributed under the terms and conditions of the Creative Commons Attribution (CC BY) license (https://creativecommons.org/licenses/by/4.0/).

1. Introduction

The application of radiocarbon dating techniques to architectural materials offers unique insights into the historical contexts of ancient structures [1]. In this study, we present a comprehensive analysis of historical mortar and plaster samples from the San Salvatore—Massino Visconti complex located in Piedmont, Northern Italy. This complex, with its rich historical background dating back to the Benedictine Abbey of St. Gallo and subsequent transformations under the Visconti family and Augustinian hermits, provides an intriguing archaeological context for understanding the construction practices and material compositions prevalent in the region from the 12th to 16th centuries.

The analysis involved the examination of several mortar samples and one charcoal sample collected from various areas within the lower chapels of the San Salvatore complex. Through a multi-analytical approach, including mineralogical, compositional, and microstructural analyses, we identified significant mineral phases such as hydromagnesite and magnesite within the mortar samples, indicating the use of a magnesian binder mortar [2,3]. The magnesian binder mortar challenges conventional radiocarbon dating methods due to the slower carbonation reaction of magnesian lime compared to calcitic lime [4,5].

Indeed, these mineral phases in the mortar mix might slightly shift the dating towards more recent dates due to the slower carbonation reaction of magnesian mortars when compared to usual calcitic ones. Magnesium oxide (MgO) from the calcination of magnesian carbonates is less reactive with water than is calcium oxide (CaO), and the former has a lower carbonation kinetic. Typically, the carbonation of magnesian lime does not exceed 60% (compared to 95% for calcium lime), so calcium hydroxide transforms into calcite, while most of the magnesium hydroxide either remains uncarbonated or carbonatates slowly and partially to form compounds like hydromagnesite [6–9]. Furthermore, the identification of LDH (Layer Double Hydroxides) phases like hydrotalcite is crucial for radiocarbon dating. LDH minerals form as a result of a pozzolanic reaction and have a high capacity to fix carbonate anions (CO_3^{-2}) into their crystalline structure, introducing contamination from younger carbon into the system, which would shift the radiocarbon dates [10–13].

Our study comprised a complete characterization of the binding materials through different analytical techniques, such as X-ray powder diffraction (XRPD), optical microscopy (OM), and scanning electron microscopy coupled with energy-dispersive spectroscopy (SEM-EDS), to address these challenges. Furthermore, a wet gravimetric separation for the extraction of a fine fraction (SG) mainly composed of the mortar binder was carried out and the SG was characterized by XRPD to investigate the presence of contaminants. This preliminary characterization is necessary for a reliable radiocarbon dating of samples [12,14,15].

Since the analyzed samples exhibited phases considered contaminants for radiocarbon dating purposes (such as LDHs), an additional purification step was carried out through thermal treatment at 550 °C for 30 min under vacuum conditions, aiming to release the incorporated CO_3^{-2} by collapsing its chemical structure. The temperature selected was based on the thermal decomposition temperatures of LDHs and carbonates. In the case of Mg-carbonates, the primary components of ancient magnesian mortars, an endothermic decomposition process occurs, releasing water and CO_2 within a temperature range varying approximately between 220 and 550 °C. The thermal decomposition mechanisms of LDHs have been extensively studied, and typically exhibit a three-step mass loss pattern, namely, dehydration (25–280 °C), dehydroxylation (280–400 °C), and anion expulsion (>400 °C), resulting in the gradual collapse of the double-layered structure [13,16–19].

By successfully eliminating the contaminant fractions, we achieved reliable radiocarbon ages that align with the historical timeline of the San Salvatore complex. Furthermore, our findings shed light on the viability of radiocarbon dating for magnesian mortars, a previously overlooked aspect of archaeological research.

Through this investigation, we aim to contribute to a deeper understanding of the construction history and material compositions of the San Salvatore complex, offering valuable insights into the architectural structures. Additionally, our study contributes to further research into radiocarbon dating of magnesian mortars, potentially refining the approaches used in archaeological dating methods for similar historical sites worldwide.

2. Historical Background and Architectural Description (Construction Phases)

The historical study of the church was conducted by a team of architects and historians who provided a report with the reconstruction of the historical and architectural events that affected the monastery, aimed at the restoration interventions scheduled to take place in the following months [20,21].

The full jurisdiction of the Benedictine abbey of St. Gallo over Massino lasted over two centuries, suggesting the presence of Benedictine monks. Although there is little information as to this period of religious revival, marked by the proliferation of churches, from the 11th century onwards, churches dedicated to Jesus Christ, St. Michele, St. Quirico, St. Margherita, and St. Maria Maddalena flourished. The 12th century witnessed the emergence of the Visconti family's control, leading to conflicts and an eventual decline in

the abbey's influence. The site saw subsequent changes, passing to the Augustinian hermits in 1499 and eventually becoming part of the Massino parish in 1660.

The ecclesiastical complex of San Salvatore (Figure 1), situated on Mount San Salvatore, underwent numerous transformations over the centuries, reflecting its irregular architectural layout resulting from the steep terrain. It consists of the church of San Salvatore, dedicated to the Madonna della Cintura, the two chapels dedicated to the Crucifixion and St. Uguccione, and the three chapels dedicated to San Quirico, Santa Margherita, and Maria Maddalena. The oldest part of the complex includes the churches dedicated to San Salvatore and San Quirico, dating back to the 12th century. Later additions include the chapel of Santa Margherita and the upper chapel of Maddalena, showcasing a blend of architectural styles from the Romanesque to the Gothic periods. The Augustinians took charge in the 15th century, overseeing further modifications, including the construction of the bell tower and the reorientation of the church's altar. The 1499 renovation led by Frate Ippolito da Campo repurposed architectural elements, including what became the entrance portal of the 20th century facade, revealing the existence of a portico supported by columns, some of which were reused for various structures, adding to the site's historical significance (Figure 2).

Throughout the 20th century, various restoration and renovation projects were carried out at the site, including interior works, roof repairs, paving installations, and restorations of specific architectural features and chapels. These interventions were aimed at preserving and enhancing the structural integrity and historical significance of the complex.

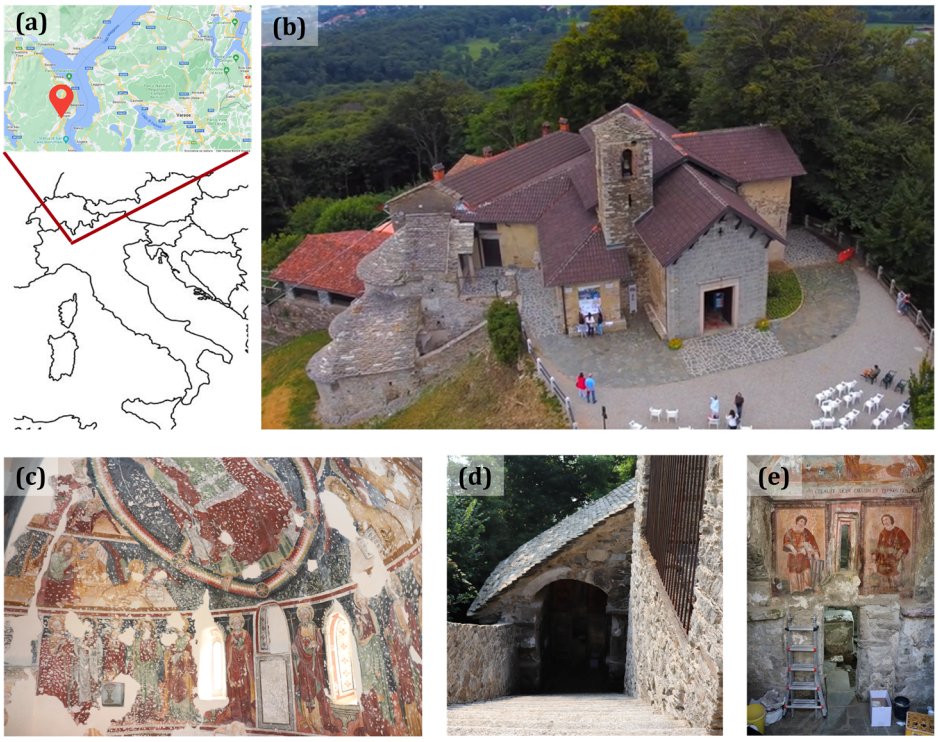


Figure 1. Complex of San Salvatore. (**a**) Position of Massino Visconti, Northen Italy. (**b**) Panoramic view of the entire complex. (**c**) Frescoes from the fifteenth century depicting a procession of the Apostles around Christ, enclosed in a tricolored mandorla, preserved in the oldest chapel of the Benedictines in the church of San Salvatore. This chapel was commissioned by Lancillotto dei Visconti, feudal lords of Massino, and executed by Giovanni De Campo. (**d**) Staircase, known as the Holy Stairs, which provides access to (**e**) the lower chapels.



Figure 2. Map of the entire San Salvatore complex, along with the construction phases occurring over the past several centuries. 1. Church of San Salvatore, 2. Chapel of the Maddalena, 3. Chapel of San Quirico, 4. Chapel of Santa Margherita, 5. Chapel of the Crucifixion, and 6. Chapel of Saint Uguccione.

3. Materials and Methods

The sampling campaign was conducted at the end of July 2020 in collaboration with Dr. Paolo Lampugnani, an archaeologist from Pandora Archeologia (Veruno, Italy). Mortar samples and one charcoal sample within a mortar were collected from various sampling areas in the lower chapels of the San Salvatore complex. According to the recommendations of the archaeologists and architects overseeing the restoration and recovery project of the complex and given the significance of the samples and their macroscopic characteristics, a selection of samples was made, as shown in Figure 3 and in Table 1, where the types of analyses performed for each sample are reported.

Table 1. List of the samples collected, with sampling area, material type, and archaeometric analysis conducted for each of the selected samples.

Sample Code	Area	Material	Note	XRPD	OM	SEM-EDX	SG	XRPD_SG	^{14}C
MV_SS_01	A	Mortar/Plaster	Deeper layer, scratch coat	x	x	x	x	x	x
MV_SS_01_C	A	Charcoal	Charcoal in the mortar						x
MV_SS_02	A	Mortar/Plaster	Finish coat layer of the scratch coat (white in color)	x	x	x	x	x	x
MV_SS_03	A	Mortar/Plaster							
MV_SS_04	A	Mortar/Plaster							
MV_SS_05	B	Mortar/Plaster	1st layer						
MV_SS_06	B	Mortar/Plaster	2nd layer						
MV_SS_07	B	Mortar/Plaster	1st preparatory layer	x	x	x	x	x	x
MV_SS_08	C	Plaster	Fresco dated 1450	x	x	x	x	x	x
MV_SS_09	C	Mortar/Plaster	White surface layer of the dome						
MV_SS_10	C	Mortar/Plaster	White above the inscription 1541	x	x	x	x	x	x

XRPD: X-ray powder diffraction; OM: optical microscopy; SEM-EDX: scanning electron microscopy; SG: gravimetric separation of the binder fraction; XRPD_SG: X-ray powder diffraction of the binder fraction; ^{14}C: radiocarbon dating.

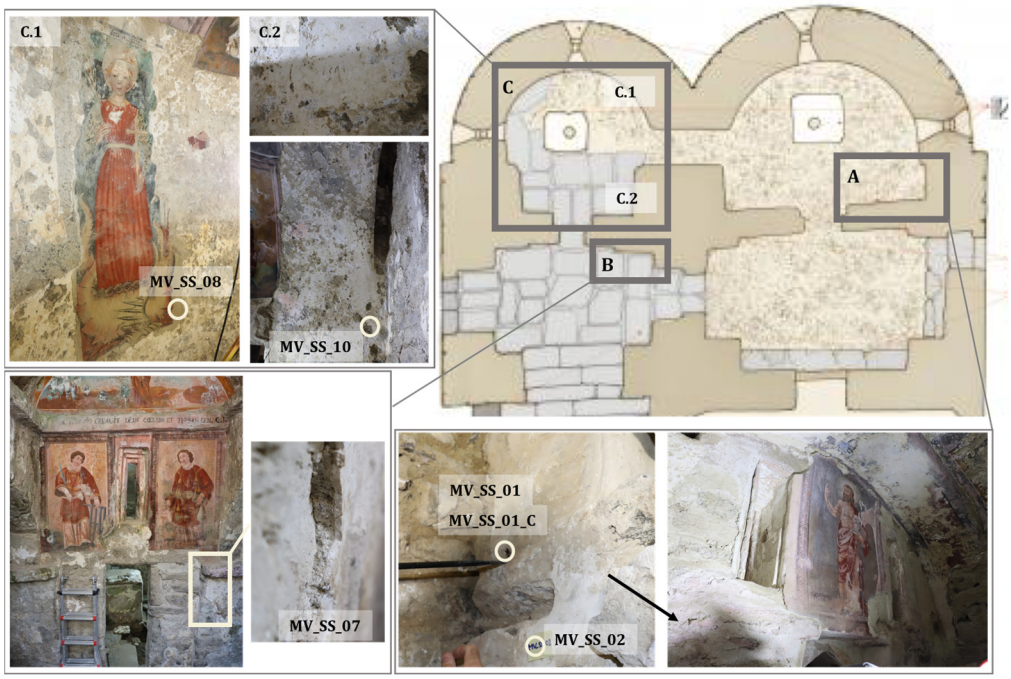


Figure 3. Map of the lower chapels of the San Salvatore complex. A. Sampling area A, the Chapel of Saint Quirico, where the samples MV_SS_01, MV_SS_01_C, and MV_SS_02 were collected. B. Sampling area B, at the entrance of the chapel of Saint Margherita, where the sample MV_SS_07 was collected. C. Sampling area C, the Chapel of Saint Margherita, where the samples MV_SS_08 (from the frescos dated to 1450, C.1) and MV_SS_10 (close to the graffito dated "1541", C.2) were collected.

The analytical methodology consisted of several distinct phases: (i) chemical–mineralogical characterization; (ii) purification procedures; (iii) characterization of extracted fine powder; (iv) sample treatment; and (v) final radiocarbon dating [14,15,22]. The characterization and separation procedures were applied at the CIRCe Centre in Padua, Italy, in the department of Geosciences of the University of Padova, while graphitization and AMS measurements were performed at the CIRCE Laboratory, Department of Mathematics and Physics, Università degli Studi della Campania, in Caserta, Italy.

Petrographic analyses were carried out using optical microscopy (OM) on 30 µm thin-sections, utilizing a Nikon Eclipse ME600 microscope (Tokyo, Japan) equipped with a Canon EOS 600D Digital single-lens reflex camera (Tokyo, Japan). Thin sections coated with graphite were microstructurally and microchemically characterized using a CamScan MX2500 scanning electron microscope (SEM) (Electron Optic Services, West Orange, NJ, USA) equipped with an EDS system. Mineralogical quantitative phase analyses (QPAs) were conducted by X-ray powder diffraction (XRPD) on fine sample powders obtained through micronization. XRPD analyses were performed using a Malvern PANalytical X'Pert PRO diffractometer (Malvern, Worcestershire, UK), and data interpretation was carried out using X'Pert HighScore Plus 3.0 software by Malvern PANalytical for qualitative phase recognition, and Topas 4.1 software by Bruker (Billerica, MA, USA) for quantitative phase analysis through Rietveld refinement [23].

Purification of the mortar samples involved manual cleaning and disaggregation, followed by ultrasonic baths and wet sedimentation to separate particles [10,24]. Fine-grained particles were filtered using a vacuum pump system and 0.1 µm filters.

The filtered particles underwent XRPD analysis to assess the presence of contaminants. Samples containing LDHs and Mg-hydrates underwent thermal treatment at 550 °C for 30 min to break down the crystal structure of the mineral phases, potentially inducing errors in age determination. The residual purified fractions were collected and subsequently subjected to total digestion process in 85% orthophosphoric acid for two hours at 80 °C to convert all the carbonate material into CO_2. The charcoal found within the mortar,

MV_SS_01_C, was initially purified according to a modified ABA protocol [25,26] and then combusted to evolve the carbonaceous fraction into CO_2 for dating purposes. The CO_2 produced through combustion and/or acid digestion was later cryogenically purified by the usage of dry ice/ethanol slush and LN2, and reduced to graphite by means of the Zn sealed tube reaction protocol developed at CIRCE Lab [27], before being measured for ^{14}C isotopic ratio via Accelerator Mass Spectrometry (AMS) by run isotope fractionation correction, with blank subtraction by IAEA C1 (marble) and normalization to IAEA C2 (travertine) [28,29]. The measured radiocarbon isotopic ratios were subsequently converted to radiocarbon ages (RCages) according to the method described by Stuiver and Polach [30], and finally calibrated to absolute calendric ages by the OxCal 4.2 software [23], with the addition of the INTCAL 20 calibration curve [31,32].

4. Results and Discussion

4.1. Mortar Characterization

The selected mortar and plaster samples were analyzed using X-ray diffractometry to determine the bulk mineral composition (Table 2 and Figures S1–S5 in the Supplementary Materials). Carbonate phases such as calcite (ranging from 9 to 70%), aragonite (0.9% in sample MV_SS_01), and magnesite (abundant in samples MV_SS_02 and MV_SS_10, accounting for 11% and 17%, respectively) were identified, along with silicate phases including quartz, micas, feldspars (albite), and magnesium-rich clay minerals. Quartz, feldspars, and mica could be associated with the inert fraction of the aggregate, while calcite and magnesite may be due to both the carbonate binder fraction and the presence of carbonate sand in the aggregate. The presence of magnesium-rich phyllosilicate clay components (chlorite and montmorillonite) suggests an intentional or accidental addition to the mortar mix. The mineral composition also revealed the presence of hydrotalcite-like phases (magnesium hydroxy-aluminates, LDHs), ranging from 0.1% to 3.8%, associated with abundant fractions of amorphous phases (up to 30%), indicating partial hydraulic reaction processes. Reactive silicate components likely reacted to form complex paracrystalline products such as hydrated calcium and magnesium silicates and aluminates, as well as LDHs due to hydraulic reactions. These reaction products can trap carbon dioxide, introducing younger carbon into the system, thus compromising radiocarbon analyses, causing the dating to be closer to the present time. Sample MV_SS_02 is indicative of the white finishing surface layer, characterized by high contents of calcite and magnesite and small fractions of silicate aggregate, which is consistent with the mineral composition of an internal lime-plaster layer. Sample MV_SS_10 exhibits high content levels of magnesite, calcite and hydromagnesite, in addition to amorphous phases, which is indicative of a magnesian lime plaster with reaction phases (LDH) resulting from partial hydraulic reactions. The presence of magnesite and/or hydromagnesite is indicative of the use of a magnesian-type binder characterized by good binding capacity and mechanical strength.

Table 2. Quantitative XRPD analysis, expressed as %wt of the mineral phases identified in the analyzed samples.

Samples	Calcite	Aragonite	Magnesite	Quartz	Albite	Micas	Mg-Clay	HydroMg	LDH	Amorp.
MV_SS_01	21.0	0.9	0.4	20.2	5.8	12.9	6.7	0.0	3.8	28.2
MV_SS_02	70.2	0.0	11.0	4.2	1.6	4.1	0.9	0.0	1.8	6.3
MV_SS_07	9.1	0.0	1.7	27.9	7.3	15.3	6.4	0.0	2.8	29.2
MV_SS_08	22.8	0.0	0.0	27.8	7.6	7.4	1.7	16.9	0.1	15.8
MV_SS_10	29.7	0.0	17.5	0.1	0.0	1.7	0.0	19.5	1.0	30.5

Mg-Clay: magnesian clays; HydroMg: hydromagnesite; LDH: layer double hydroxide, as hydrotalcite and hydrocalumite phases; Amorp.: amorphous content.

From a mineral-petrographic perspective, optical microscopy investigations (Figure 4) revealed that samples MV_SS_01, MV_SS_07, and MV_SS_08 are mortars with binder/aggregate ratios of 1:1. The binder matrix exhibits a micritic texture with high interference colors typical of calcite and zones of darker coloration which can be attributed to low-crystallinity phases. The inert fraction primarily consists of quartzites, feldspars, and mica, with angular clasts characteristic of a fluvial aggregate with minimal erosion. In samples MV_SS_01 and MV_SS_07, the inert fraction appears poorly selected, with grain sizes up to 10 mm in length distributed non-uniformly and non-oriented within the mix, while in sample MV_SS_08, the aggregates are moderately selected and more uniformly distributed.

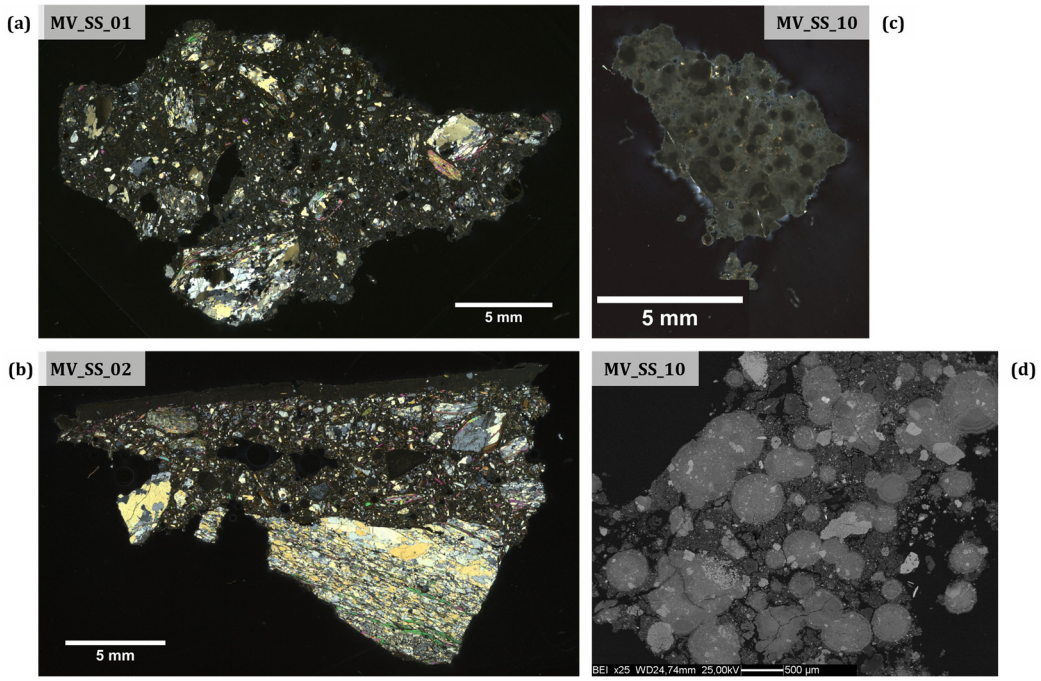


Figure 4. Optical microscopy micrographs of representative samples in polarized transmitted light (TL) and crossed nicols. (**a**,**b**) are MV_SS_01 and MV_SS_02, respectively. (**c**,**d**) Visible magnesium-enriched areas in the dolomitic lime mortar MV_SS_10 sample: (**c**) thin-section photomicrograph of diffuse brownish patches in the binder, (**d**) photomicrograph of the same sample using a backscattering electron image (BSI).

Samples MV_SS_02 and MV_SS_10 refer to surface layers of internal plaster, and optical microscopy images reveal low-interference colors typical of magnesian mortars and amorphous phases. Inert fractions are not evident, which is consistent with XRPD mineralogical investigations detecting small fractions of aggregate-related phases.

Areas with low-interference colors may be attributed to hydromagnesite (a partially carbonated phase of magnesium hydroxide) [2,33]. The magnesian phase may be separate from the calcic phase due to magnesium hydroxide's slower carbonation rate compared to calcium hydroxide. In sample MV_SS_10, hydromagnesite is visible in subspherical "ghost" forms devoid of internal structure (see Figure 4c,d).

Observations using electron microscopy (Figure 5) highlighted the nature of the binders used in these mortars. Samples MV_SS_01 and MV_SS_07 are very similar to each other in both microstructure and the chemical composition of the binder matrix and lime nodules. Microchemical analyses using EDS on the matrices reveal high levels of calcium (Ca) associated with magnesium (Mg), silicon (Si), and aluminum (Al). This composition may be related to complex LDH phases formed through hydraulic reactions between lime and reactive clay phases in a highly basic and magnesium-rich environment (both the clay and the lime used may have released magnesium into the system). In particular, the high magnesium content in the matrix may be linked to the use of a slightly magnesian

lime, but is mainly due to the high content of phyllosilicates, which are visible in the SEM micro-images and recognizable by their lamellar appearance. Microchemical analyses of the lime nodules reveal a calcic chemical composition, indicating the use of aerial lime binder. Moreover, accumulations of M-S-H, magnesium-silicate-hydrates, are evident (Figure 5a, point 1), and are properly recognized in ancient mortars [12,34–39]. The formation of M-S-H phases is promoted under certain conditions in high-pH reactive environments characterized by high magnesium activity, through the interaction of magnesium with silica, or, sometimes, also with alumina (M-A-S-H). Although they are not easily detectable by XRPD due to their disordered and paracrystalline structure, they can be diagnosed based on the chemical components present and their relative ratios [40–42].

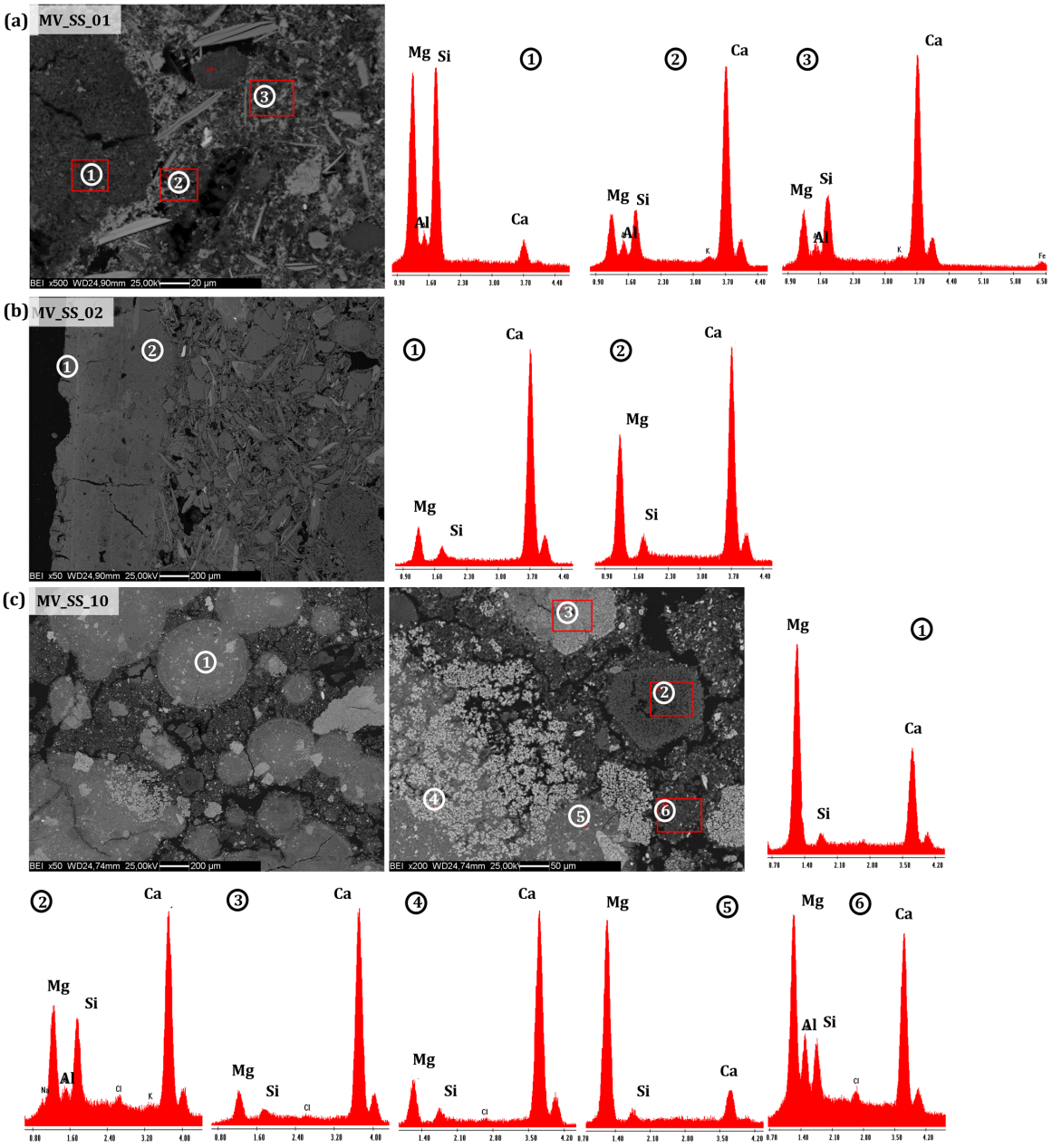


Figure 5. SEM-EDS analyses of representative mortar samples. Backscattered electron images (BSI) and chemical analyses (EDS). (**a**) MV_SS_01: (1) lump of M-S-H, magnesium-silicate-hydrate; (2) and (3), microanalyses of the matrix. (**b**) MV_SS_02: (1) and (2), microanalyses of the matrix of the plaster layer. (**c**) MV_SS_10: EDS microanalyses of (1) hydromagnesite "ghost", (2) lump, (3) carbonate aggregate, (4) calcic carbonate precipitation, (5) magnesite, and (6) matrix.

Sample MV_SS_02 (Figure 5b) appears to be a homogeneous layer of fatty mortar with a chemical composition rich in Ca associated with varying proportions of Mg and Si, which is consistent with a mineral composition predominantly comprising 70% calcite, 10% magnesite, and 1.8% hydrotalcite (LDH). The fresco sample (MV_SS_08) exhibits a matrix microstructure that is less compact and a chemical composition mainly composed of Ca associated with Mg, which is attributable to the presence of calcite and hydromagnesite, as identified in the XRPD analysis. Finally, sample MV_SS_10 prominently displays hydromagnesite "ghosts" characterized by high Mg content and a typical subspherical appearance devoid of internal structure (Figure 5c) [3]. Additionally, the matrix mainly consists of Ca, Mg, and Si, which is attributable to the presence of calcite and magnesite associated with paracrystalline phases of hydrated magnesium silicates and LDH, consistent with the mineral composition revealed by XRPD.

4.2. Binder Fraction Characterization

The selected samples were treated in order to obtain the fine binder fractions (SGs) via wet gravimetric preparation, which were then analyzed using XRPD (Table 3 and Figures S6–S10 in the Supplementary Materials). The results show the presence of calcite (ranging from 19 to 82%), magnesite (from 1 to 15%), abundant amorphous phases (up to 59%), hydrotalcite (LDH, abundant in sample MV_SS_07), aragonite (3% in sample MV_SS_01 only), phyllosilicates (mica and magnesium-rich clays), and hydromagnesite (abundant in samples MV_SS_08 and MV_SS_10). The aggregate fraction, primarily composed of quartz and feldspars (albite), was completely removed during the binder extraction procedure. The presence of aragonite (a metastable polymorph of calcium carbonate) in sample MV_SS_01 could be associated with the alteration phenomena of paracrystalline phases formed during pozzolanic reaction and/or may be due to the carbonation process of calcium oxide [43]. The indication of the presence of biogenic aragonite is not reliable, since no evidence of shells or similar aggregates was found in the macroscopic and microscopic investigations.

Table 3. Quantitative XRPD analyses, expressed as %wt of the mineral phases identified in the analyzed samples.

Samples		Calcite	Arag.	Magnesite	Micas	Mg-Clays	HydroMg	LDH	Amorp.
MV_SS_01	SG	30.7	3.0	0.0	7.4	0.0	0.0	0.1	58.9
MV_SS_02	SG	82.1	0.0	1.4	3.3	0.0	0.0	0.0	13.2
MV_SS_07	SG	25.6	0.0	14.2	5.0	2.1	0.0	4.8	48.3
MV_SS_08	SG	19.0	0.0	2.7	0.0	8.4	16.9	0.0	53.0
MV_SS_10	SG	22.4	0.0	15.4	0.0	15.7	9.9	2.1	34.6

Mg-Clay: magnesian clays; HydroMg: hydromagnesite; LDH: layer double hydroxide, as hydrotalcite and hydrocalumite phases; Amorp.: amorphous content.

The identification of LDH phases such as hydrotalcite is crucial for radiocarbon dating purposes; LDH minerals form as a result of the pozzolanic reaction and have a high capacity to fix carbonate anions (CO_3^{-2}) into their crystalline structure, introducing contamination from younger carbon into the system, which may shift the radiometric dates towards later dates.

To address these issues, in order to eliminate these radiocarbon contaminants, purification methods for the mortar matrix were developed, utilizing a thermal treatment at 550 °C (a temperature at which the decomposition of LDH phases occurs but not that of the calcium carbonate in the binder fraction, which decomposes at higher temperatures, approximately 800–850 °C [44]).

4.3. Mortar Radiocarbon Dating

Once the binder fraction was purified through thermal heating and reduced to graphite (C), the samples underwent measurement of the ^{14}C isotopic ratio using Accelerator Mass Spectrometry (AMS). The radiocarbon dates obtained from the mortar and plaster samples, as well as from the charcoal sample (MV_SS_01_C) collected within mortar MV_SS_01, are reported in Table 4 and Figure 6.

Table 4. Radiocarbon dating results of the mortar samples (SGs) and the charcoal fragments found in the mortar sample, reporting calibrated calendar ages in the ranges of 1σ and 2σ.

Lab Code	Sample Code	Fraction	^{14}C Age	Cal AD Age Range (2σ)	Cal AD Age Range (1σ)	Reliable Age?
DSH10245_SG	MV_SS_01	SG_01	749 ± 50	AD 1179–1387	AD 1227–1289	Yes
DSH10222_CH	MV_SS_01_C	charcoal	867 ± 19	AD 1159–1223	AD 1175–1216	Yes
DSH10213_SG	MV_SS_02	SG_01	768 ± 21	AD 1225–1280	AD 1232–1278	Yes
DSH10214_SG	MV_SS_07	SG_01	635 ± 37	AD 1287–1398	AD 1298–1393	Yes
DSH10215_SG	MV_SS_08	SG_01	246 ± 25	AD 1526–1800	AD 1641–1795	No
DSH10216_SG	MV_SS_10	SG_01	403 ± 23	AD 1440–1620	AD 1447–1487	Yes

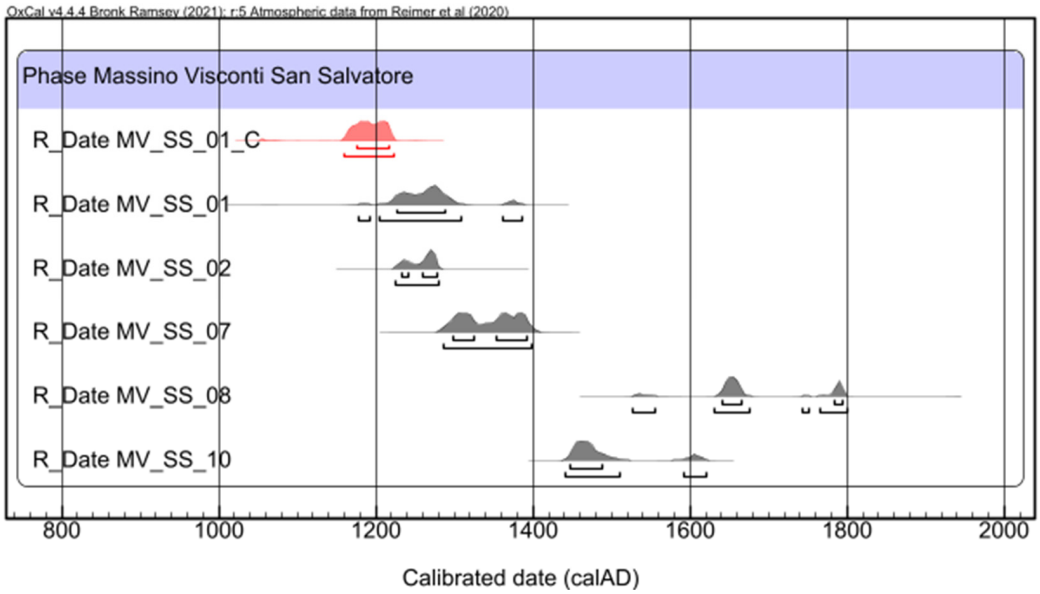


Figure 6. Calibrated dates of the ^{14}C measurements of mortar samples and charcoal (in red) by means of OxCal 4.4 [45] and the IntCal 20 calibration curve [31].

Samples MV_SS_01, MV_SS_01_C, and MV_SS_02 were taken from the chapel of San Quirico and originate, respectively, from the mortar, a fragment of charcoal within the mortar (01), and the white finishing layer. The calibrated ages place the samples between the late 12th and 13th centuries and are reliable and in agreement with each other.

The sample taken at the entrance of the chapel of Santa Margherita (MV_SS_07) yields a calendar age between 1300 and 1400. The observed age aligns with archaeological hypotheses placing the construction of the celebratory apse at Santa Margherita within the 13th or 14th century, and thus later than the oldest part of the church, which is dedicated to San Salvatore, as well as the portion dedicated to San Quirico (11th–12th centuries). Within the same chapel, sample MV_SS_10 was taken from the white finishing layer adjacent to the inscription "1541", indicating that the plaster should precede this date. The radiocarbon results place the sample between 1440 and 1511 (83%) and 1591–1620 (12%) (Figure S11), calendar AD age range (2σ), so, given the inscription, we can assume that the finishing layer

was executed between 1440 and 1511. Therefore, the result is consistent with the data. The only date that appears unreliable is related to the sample taken from the margin of a fresco inside the chapel of Santa Margherita (sample MV_SS_08). According to historical sources, the fresco could be attributed to the same painter who created the fresco cycle inside the church of San Salvatore and the chapel of the Crucifixion, during the period when the care of the complex was entrusted to the Augustinians (around the mid-1400s). The mortar sample was taken at the edge of the fresco itself, without involving the painted layer, out of respect for the artwork. Therefore, the analysis for the date obtained (calibrated age, 1526-1800 AD 2σ) might have been contaminated by subsequent restoration interventions performed during the 20th century.

5. Conclusions

Our findings highlight the potential of radiocarbon dating for evaluating magnesian mortars, an aspect that has previously been overlooked in archaeological investigations. The multi-analytical study conducted on mortar and plaster samples selected from the complex of the church of San Salvatore—Massino Visconti (NO) has allowed the characterization of their main compositional, mineralogical, and microstructural characteristics. Furthermore, by successfully isolating and purifying the binder fractions, we achieved reliable radiocarbon ages that align with the historical timeline of the San Salvatore complex.

The mortar samples MV_SS_01, MV_SS_07, and MV_SS_08 appear to be slightly magnesian air limes with a mineralogical composition compatible with locally available raw materials. The magnesian components (magnesite and hydromagnesite) identified in the examined samples contribute to ensuring greater homogeneity between binder and aggregate, resulting in mortars with improved mechanical strength. Similarly, the samples from the white finishing layers (MV_SS_02 and MV_SS_10) are made with a fat lime mortar based on magnesian lime.

The binder used is therefore an air lime of calcareous and magnesian composition, and the matrix consists of calcium carbonate, magnesium, and elements (such as silicon and aluminum) indicative of a partial hydraulic reaction with the formation of secondary phases (LDH and M-S-H), favored by the occurrence of large amounts of magnesium derived from both the lime itself and the magnesium-rich clay fraction.

The gravimetric separation of the binder fraction and subsequent mineralogical characterization allowed the selection of the datable binder fraction and the identification of any contaminating phases for radiocarbon dating. LDH phases capable of trapping carbon dioxide over time, and thereby introducing younger carbon into the system, were identified. The purification process carried out by thermal treatment resulted in the collapse of the LDH structure and the elimination of trapped CO_2. Consequently, the radiocarbon dates obtained are scientifically reliable and consistent with the historical interpretations provided by the studies conducted, except for the MV_SS_08 sample of the fresco inside the chapel of Santa Margherita, as that sampling likely included part of subsequent restorations.

The samples selected in the oldest chapel of the San Salvatore complex, the chapel of San Quirico, show radiocarbon ages ranging from 1150 to 1300 (MV_SS_01, MV_SS_01_C, and MV_SS_02). The sample in the entrance wall of the chapel of Santa Margherita (MV_SS_07), built about a century after the adjacent chapel, is dated between 1300 and 1400. Finally, the sample of the finishing layer inside the same chapel, consistent with the date of the assignment to the Augustinians (1450) and preceding an inscription on the same (1541), is likely dated to between 1440 and 1511.

Supplementary Materials: The following supporting information can be downloaded at: https://www.mdpi.com/article/10.3390/app14219899/s1. Figure S1. XRPD patterns of the bulk sample MV_SS_01. The main diffraction peaks of the mineral phases are highlighted. Figure S2. XRPD patterns of the bulk sample MV_SS_02. The main diffraction peaks of the mineral phases are highlighted. Figure S3. XRPD patterns of the bulk sample MV_SS_07. The main diffraction peaks of the mineral phases are highlighted. Figure S4. XRPD patterns of the bulk sample MV_SS_08. The main diffraction peaks of the mineral phases are highlighted. Figure S5. XRPD patterns of the bulk

sample MV_SS_10. The main diffraction peaks of the mineral phases are highlighted. Figure S6. XRPD patterns of the binder-concentrated sample MV_SS_01_SG. The main diffraction peaks of the mineral phases are highlighted. Figure S7. XRPD patterns of the binder-concentrated sample MV_SS_02_SG. The main diffraction peaks of the mineral phases are highlighted. Figure S8. XRPD patterns of the binder-concentrated sample MV_SS_07_SG. The main diffraction peaks of the mineral phases are highlighted. Figure S9. XRPD patterns of the binder-concentrated sample MV_SS_08_SG. The main diffraction peaks of the mineral phases are highlighted. Figure S10. XRPD patterns of the binder-concentrated sample MV_SS_10_SG. The main diffraction peaks of the mineral phases are highlighted. Figure S11. Calibrated dates of the ^{14}C measurements of mortar sample MV_SS_10 by means of OxCal 4.4 [45] and the IntCal 20 calibration curve [31].

Author Contributions: M.S., G.R., G.A., F.T. and F.M. designed the research; G.R., M.S. and I.P. collected data and performed laboratory work; G.R., M.S. and F.M. analyzed and interpreted the data; G.R. drafted the manuscript, with contributions from all authors. All authors have read and agreed to the published version of the manuscript.

Funding: This research was funded by Don Antonio Soddu from the Parrocchia Purificazione Maria Vergine, Via F. M. Visconti, 11—28040 Massino Visconti (NO). The work was a third-party project funded by the parish priest of the church.

Institutional Review Board Statement: Not applicable.

Informed Consent Statement: Not applicable.

Data Availability Statement: The original contributions presented in the study are included in the article/Supplementary Materials, further inquiries can be directed to the corresponding author.

Acknowledgments: The authors would like to thank Soprintendenza Archeologia belle arti e paesaggio per le province di Biella Novara Verbano-Cusio-Ossola e Vercelli, Sara Mantica, Benetta Brison, Lucia Mordeglia, and Paolo Lampugnari. In particular, thanks are accorded Silvia Angiolini of *Studio Tecnico Architetti Associati Vecchi E Angiolini* for sharing all the historical and architectural information and for her availability and enthusiasm.

Conflicts of Interest: The authors declare no conflicts of interest. The funders had no role in the design of the study; in the collection, analyses, or interpretation of data; in the writing of the manuscript; or in the decision to publish the results.

References

1. Urbanová, P.; Boaretto, E.; Artioli, G. The State-of-the-Art of Dating Techniques Applied to Ancient Mortars and Binders: A Review. *Radiocarbon* **2020**, *62*, 503–525. [CrossRef]
2. Pecchioni, E.; Fratini, F.; Cantisani, E. *Le Malte Antiche e Moderne tra Tradizione ed Innovazione*; Patron Editore: Bologna, Italy, 2008.
3. Dheilly, R.M.; Bouguerra, A.; Beaudoin, B.; Tudo, J.; Queneudec, M. Hydromagnesite development in magnesian lime mortars. *Mater. Sci. Eng. A* **1999**, *268*, 127–131. [CrossRef]
4. Hartshorn, H. Dolomitic Lime Mortars: Carbonation Complications and Susceptibility to Acidic Sulfates. Ph.D. Dissertation, Columbia University, New York, NY, USA, 2012.
5. Pesce, G. *Radiocarbon Dating of Lime Lumps: Current and Future Challenges*; Archeol dell'Architettura; All'Insegna del Giglio s.a.s.: Florence, Italy, 2019; pp. 19–26.
6. Lanas, J.; Alvarez, J.I. Dolomitic limes: Evolution of the slaking process under different conditions. *Thermochim. Acta* **2004**, *423*, 1–12. [CrossRef]
7. Montoya, C.; Lanas, J.; Arandigoyen, M.; Navarro, I.; García Casado, P.J.; Alvarez, J.I. Study of ancient dolomitic mortars of the church of Santa Maŕia de Zamarce in Navarra (Spain): Comparison with simulated standards. *Thermochim. Acta* **2003**, *398*, 107–122. [CrossRef]
8. Lubelli, B. Simulation of Self-Healing of Dolomitic Lime Mortar. 2014. Available online: https://www.researchgate.net/publication/254756304_Simulation_of_self-healing_of_dolomitic_lime_mortar (accessed on 21 October 2024).
9. Adriano, P.; Santos Silva, A.; Veiga, R.; Mirão, J.; Candeias, A.E. Microscopic characterisation of old mortars from the Santa Maria Church in Évora. *Mater. Charact.* **2009**, *60*, 610–620. [CrossRef]
10. Ricci, G.; Secco, M.; Marzaioli, F.; Terrasi, F.; Passariello, I.; Addis, A.; Lampugnani, P.; Artioli, G. The Cannero Castle (Italy): Development of Radiocarbon Dating Methodologies in the Framework of the Layered Double Hydroxide Mortars. *Radiocarbon* **2020**, *62*, 617–631. [CrossRef]
11. Ponce-Antón, G.; Ortega, L.A.; Zuluaga, M.C.; Alonso-Olazabal, A.; Solaun, J.L. Hydrotalcite and hydrocalumite in mortar binders from the medieval castle of portilla (Álava, north Spain): Accurate mineralogical control to achieve more reliable chronological ages. *Minerals* **2018**, *8*, 326. [CrossRef]

12. Ricci, G.; Secco, M.; Addis, A.; Pistilli, A.; Preto, N.; Brogiolo, G.P.; Arnau, A.C.; Marzaioli, F.; Passariello, I.; Terrasi, F.; et al. Integrated multi-analytical screening approach for reliable radiocarbon dating of ancient mortars. *Sci. Rep.* **2022**, *12*, 3339. [CrossRef]
13. Artioli, G.; Secco, M.; Addis, A.; Bellotto, M. Role of Hydrotalcite-type layered double hydroxides in deleyed pozzolanic reactions and ther bearing on mortar dating. In *Cementitious Materials. Composition, Properties, Application*; Walter de Gruyter GmbH: Berlin, Germany, 2017; pp. 147–158.
14. Ricci, G.; Secco, M.; Marzaioli, F.; Passariello, I.; Terrasi, F.; Artioli, G. New strategies in mortar characterization and radiocarbon dating. In Proceedings of the 2019 IMEKO TC4 International Conference Metrology Archaeology Cultural Heritage, MetroArchaeo 2019, Florence, Italy, 4–6 December 2019.
15. Artioli, G.; Barone, S.; Fedi, M.; Galli, A.; Liccioli, L.; Martini, M.; Marzaioli, F.; Maspero, F.; Panzeri, L.; Passariello, I.; et al. Characterization and Selection of Mortar Samples for Radiocarbon Dating in the Framework of the MODIS2 Intercomparison: Two Compared Procedures. *Radiocarbon* **2024**, 1–14. Available online: https://www.cambridge.org/core/product/identifier/S0033822224000031/type/journal_article (accessed on 1 March 2024). [CrossRef]
16. Stanimirova, T.; Vergilov, I.; Kirov, G.; Petrova, N. Thermal decomposition products of hydrotalcite-like compounds: Low-temperature metaphases. *J. Mater. Sci.* **1999**, *34*, 4153–4161. [CrossRef]
17. Roelofs, J.C.A.A.; van Bokhoven, J.A.; van Dillen, A.J.; Geus, J.W.; de Jong, K.P. The Thermal Decomposition of Mg-Al Hydrotalcites: Effects of Interlayer Anions and Characteristics of the Final Structure. *Chem.—A Eur. J.* **2002**, *8*, 5571–5579. [CrossRef]
18. Pérez-Ramírez, J.; Abelló, S. Thermal decomposition of hydrotalcite-like compounds studied by a novel tapered element oscillating microbalance (TEOM): Comparison with TGA and DTA. *Thermochim. Acta* **2006**, *444*, 75–82. [CrossRef]
19. Bhattacharjya, D.; Selvamani, T.; Mukhopadhyay, I. Thermal decomposition of hydromagnesite effect of morphology on the kinetic parameters. *J. Therm. Anal. Calorim.* **2012**, *107*, 439–445. [CrossRef]
20. Grassi, V. *Appunti di Storia Massinesi*; Administration of Massino Visconti: Massino Visconti, Italy, 2004.
21. Frigerio, P.; Pisoni, P.; Grassi, V. *Le Più Antiche Chiese di Massino e i Problemi Della Loro Storia*; Novarien: Rome, Italy, 1983.
22. Marzaioli, F.; Lubritto, C.; Nonni, S.; Passariello, I.; Capano, M.; Terrasi, F. Mortar radiocarbon dating: Preliminary accuracy evaluation of a novel methodology. *Anal. Chem.* **2011**, *83*, 2038–2045. [CrossRef] [PubMed]
23. Rietveld, H.M. A profile refinement method for nuclear and magnetic structures. *J. Appl. Crystallogr.* **1969**, *2*, 65–71. [CrossRef]
24. Addis, A.; Secco, M.; Artioli, G.; Marzaioli, T.; Passariello, I.; Terrasi, F. The mortars of the excavation at the baptistery of Padua 14C dating and production technology. In *Ricerche sul Centro Episcopale di Padova–Scavi 2011–2012*; SAP Società Archeologica: Walldorf, Germany, 2017; pp. 69–83.
25. Berger, R. 14 C Dating Mortar in Ireland. *Radiocarbon* **1992**, *34*, 880–889. [CrossRef]
26. Al-Bashaireh, K.; Hodgins, G.W.L. AMS 14C dating of organic inclusions of plaster and mortar from different structures at Petra-Jordan. *J. Archaeol. Sci.* **2011**, *38*, 485–491. [CrossRef]
27. Marzaioli, F.; Borriello, G.; Passariello, I.; Lubritto, C.; de Cesare, N.; D'Onofrio, A.; Terrasi, F. Zinc reduction as an alternative method for AMS radiocarbon dating: Process optimization at CIRCE. *Radiocarbon* **2008**, *50*, 139–149. [CrossRef]
28. Terrasi, F.; De Cesare, N.; D'Onofrio, A.; Lubritto, C.; Marzaioli, F.; Passariello, I.; Rogalla, D.; Sabbarese, C.; Borriello, G.; Casa, G.; et al. High precision 14C AMS at CIRCE. *Nucl. Instrum. Methods Phys. Res. Sect. B Beam Interact. Mater. At.* **2008**, *266*, 2221–2224. [CrossRef]
29. Rozanski, K.; Stichler, W.; Gonfiantini, R.; Scott, E.M.; Beukens, R.P.; Kromer, B.; Van Der Plicht, J. The IAEA 14 C Intercomparison Exercise 1990. *Radiocarbon* **1992**, *34*, 506–519. [CrossRef]
30. Stuiver, M.; Polach, H.A. Discussion Reporting of 14 C Data. *Radiocarbon* **1977**, *19*, 355–363. [CrossRef]
31. Reimer, P.J.; Austin, W.E.; Bard, E.; Bayliss, A.; Blackwell, P.G.; Ramsey, C.B.; Butzin, M.; Cheng, H.; Edwards, R.L.; Friedrich, M.; et al. The IntCal20 Northern Hemisphere Radiocarbon Age Calibration Curve (0–55 cal kBP). *Radiocarbon* **2020**, *62*, 725–757. [CrossRef]
32. Bronk Ramsey, C. Bayesian Analysis of Radiocarbon Dates. *Radiocarbon* **2009**, *51*, 337–360. [CrossRef]
33. Diekamp, A.; Konzett, J.; Mirwald, P.W.; Tyrol, S. Magnesian Lime Mortars—Identification of Magnesium-Phases. In Proceedings of the 12th Euroseminar on Microscopy Applied to Building Materials, Dortmund, Germany, 12–15 December 2009; pp. 309–318. Available online: https://www.researchgate.net/publication/236875128 (accessed on 25 August 2021).
34. Dilaria, S.; Secco, M.; Bonetto, J.; Ricci, G.; Artioli, G. Making Ancient Mortars Hydraulic. How to Parametrize Type and Crystallinity of Reaction Products in Different Recipes. In *Conservation and Restoration of Historic Mortars and Masonry Structures*; HMC 2022. RILEM Bookseries; Springer: Cham, Switzerland, 2023; Volume 42, pp. 6–52. [CrossRef]
35. Bechor, B.; Sivan, D.; Miko, S.; Hasan, O.; Grisonic, M.; Rossi, I.R.; Lorentzen, B.; Artioli, G.; Ricci, G.; Ivelja, T.; et al. Salt pans as a new archaeological sea-level proxy: A test case from Dalmatia, Croatia. *Quat. Sci. Rev.* **2020**, *250*, 106680. [CrossRef]
36. Beltrame, C.; Medas, S.; Mozzi, P.; Ricci, G. Roman 'Well-cisterns', Navigational Routes, and Landscape Modifications in the Venice Lagoon and Northeastern Adriatic. *Int. J. Naut. Archaeol.* **2023**, *52*, 133–157. [CrossRef]
37. Alonso-Olazabal, A.; Ortega, L.A.; Zuluaga, M.C.; Ponce-Antón, G.; Echevarría, J.J.; Fernández, C.A. Compositional characterization and chronology of roman mortars from the archaeological site of arroyo de la dehesa de velasco (Burgo de osma-ciudad de osma, Soria, Spain). *Minerals* **2020**, *10*, 393. [CrossRef]
38. Ponce-Antón, G.; Zuluaga, M.C.; Ortega, L.A.; Mauleon, J.A. Petrographic and chemical-mineralogical characterization of mortars from the cistern at amaiur castle (Navarre, Spain). *Minerals* **2020**, *10*, 311. [CrossRef]

39. Secco, M.; Dilaria, S.; Bonetto, J.; Addis, A.; Tamburini, S.; Preto, N.; Ricci, G.; Artioli, G. Technological transfers in the Mediterranean on the verge of Romanization: Insights from the waterproofing renders of Nora. *J. Cult. Herit.* **2020**, *44*, 63–82. [CrossRef]
40. Roosz, C.; Grangeon, S.; Blanc, P.; Montouillout, V.; Lothenbach, B.; Henocq, P.; Giffaut, E.; Vieillard, P.; Gaboreau, S. Crystal structure of magnesium silicate hydrates (M-S-H): The relation with 2:1 Mg-Si phyllosilicates. *Cem. Concr. Res.* **2015**, *73*, 228–237. [CrossRef]
41. Brew, D.R.M.; Glasser, F.P. Synthesis and characterisation of magnesium silicate hydrate gels. *Cem. Concr. Res.* **2005**, *35*, 85–98. [CrossRef]
42. Secco, M.; Asscher, Y.; Ricci, G.; Tamburini, S.; Preto, N.; Sharvit, J.; Artioli, G. Cementation Processes of Roman Pozzolanic Binders from Caesarea Maritima (Israel). *Constr. Build. Mater.* **2022**, *355*, 129128. [CrossRef]
43. Toffolo, M.B.; Boaretto, E. Nucleation of aragonite upon carbonation of calcium oxide and calcium hydroxide at ambient temperatures and pressures: A new indicator of fire-related human activities. *J. Archaeol. Sci.* **2014**, *49*, 237–248. [CrossRef]
44. Cultrone, G.; Rodriguez-Navarro, C.; Sebastian, E.; Cazalla, O.; De La Torre, M.J. Carbonate and silicate phase reactions during ceramic firing. *Eur. J. Miner.* **2001**, *13*, 621–634. [CrossRef]
45. Bronk Ramsey, C. OxCal v.4.4.4 [Software]. 2021. Available online: https://c14.arch.ox.ac.uk/oxcal.html (accessed on 13 May 2023).

Disclaimer/Publisher's Note: The statements, opinions and data contained in all publications are solely those of the individual author(s) and contributor(s) and not of MDPI and/or the editor(s). MDPI and/or the editor(s) disclaim responsibility for any injury to people or property resulting from any ideas, methods, instructions or products referred to in the content.